AIAA JOURNAL
Vol. 43, No. 11, November 2005

Technical Notes

TECHNICAL NOTES are short manuscripts describing new developments or important results of a preliminary nature. These Notes should not exceed 2500 words (where a figure or table counts as 200 words). Following informal review by the Editors, they may be published within a few months of the date of receipt. Style requirements are the same as for regular contributions (see inside back cover).

Numerical Solver for Dense Gas Flows

Paola Cinnella* and Pietro M. Congedo†
Università degli Studi di Lecce, 73100 Lecce, Italy

Introduction

DENSE gas dynamics studies the dynamic behavior of gases in the dense regime, i.e., at temperatures and pressures close to the thermodynamic critical point. In such conditions, complex gasdynamic phenomena can appear in the transonic and supersonic regimes.[1] In spite of the additional complexity of the fluid response in the dense regime, the use of dense gases is not only necessary but, in some applications, advantageous. For instance, dense gas effects play a critical role in the performance of turbomachinery and heat-transfer equipment of organic Rankine cycles (ORCs).[2] This motivates the interest in developing numerical tools for the analysis and design of advanced ORC turbomachinery components.

In the past, several methods for so-called "real gas flows" have been derived. Such methods were in general tailored to deal with hypersonic reacting flows, for which the use of robust upwind numerical solvers was mandatory. Unfortunately, upwind schemes require characteristic decompositions, making their realization for complex multidimensional systems quite involved. On the other hand, for nonreacting flows of gases close to saturation conditions, governed by complex equations of state, and characterized by "exotic" but quite weak waves, the use of sophisticated characteristic decompositions is not essential. For these flows, it could be more convenient to use central schemes, which, in spite of higher numerical diffusivity, have the advantage of conceptional simplicity and low computational cost.

In the present work, a centered numerical solver for the computation of inviscid and viscous dense gas flows is developed. A third-order-accurate centered method for perfect gas flows[3] is extended to the computation of dense gases. The proposed scheme is systematically compared to a well-known second-order flux-difference splitting scheme[4] implemented within the same code. The computations are performed using either the van der Waals or the realistic Martin–Hou[5] equation of state. The scheme is then extended to the computation of viscous dense gas flows. The fluid viscosity and thermal conductivity are evaluated using thermophysical models appropriate for gases close to saturation conditions. The proposed method is validated for several inviscid and viscous flow problems involving dense gas phenomena.

Received 28 February 2005; accepted for publication 9 May 2005.

*Assistant Professor, Dipartimento di Ingegneria dell'Innovazione, via Monteroni. Member AIAA.

†Ph.D. Student, Dipartimento di Ingegneria dell'Innovazione, via Monteroni.

Dense Gases

Some heavy fluids may exhibit nonclassical phenomena in the single-phase vapor region above the upper saturation curve, i.e., the dense gas region. Their behavior is governed by the key parameter Γ, referred to as the fundamental derivative of gas dynamics,[6] which represents a measure of the rate of change of the sound speed in isentropic perturbations. If $\Gamma < 1$, the sound speed grows in isentropic expansions and falls in isentropic compressions, contrarily to what happens in "common" fluids. For perfect gases, Γ is equal to $(\gamma + 1)/2$, and always greater than 1. For heavier gases with complex molecules, Γ can be less than 1, or even than 0, for extended ranges of densities and pressures close to saturation conditions. In flow regions where $\Gamma < 0$, nonclassical gasdynamic phenomena appear in the transonic and supersonic regimes: compression shocks disintegrate, as they violate the second law of thermodynamics, whereas expansion shocks are physically admissible. Fluids which exhibit a region of negative Γ in the vapor phase are referred to as Bethe–Zel'dovich–Thompson (BZT) fluids. For transonic and supersonic BZT flows, shock waves with jump conditions close to the $\Gamma = 0$ contour have necessarily limited strength, and are much less dissipative than normal.[7]

Another important difference between dense and perfect gases is the downward curvature of the isotherms in the neighborhood of the critical point. In this region, the fluid specific heat becomes quite high, deeply affecting the development of the thermal boundary layer and its coupling with the viscous boundary layer. Moreover, in the dense gas regime the dependence of dynamic viscosity and thermal conductivity on temperature and pressure is no longer negligible, even in flows with small temperature variations. The complexity of the gas response in the dense regime can be anticipated by recalling that the viscosity of liquids tends to decrease with increasing temperature, whereas that of gases tends to increase: the dense gas regime is a transition between these two different behaviors. Similarly, the classical approximation of nearly constant Prandtl number throughout the flow cannot be used any more.

As long as the thermodynamic states are restricted to the single-phase regime, dense gas flows are governed by the Navier–Stokes equations for equilibrium, nonreacting flows. To account for dense gas effects, two gas models are considered in the present work: the van der Waals equation of state for polytropic gases, and the realistic Martin–Hou equation of state,[5] with a power law used to model the specific heat dependence on temperature. The fluid viscosity and thermal conductivity are evaluated using the method of Ref. 8. For turbulent-flow computations, we assume for simplicity that the turbulence structure is not affected by dense gas effects and adopt the classical turbulence model of Baldwin and Lomax. Similarly, lacking detailed information, a turbulent Fourier law is used for turbulent heat transfer, as usual for perfect gas flows.

Numerical Method

The main features of the proposed numerical scheme are illustrated for the one-dimensional Euler equations

$$w_t + f_x(w) = 0 \tag{1}$$

with w the conservative variable vector and $f(w)$ the flux function. On a regular mesh $x_j = j\delta x$ system (1) is first approximated using

the classical centered second-order semidiscrete scheme

$$w_t|_j + (1/\delta x)\delta\mu f|_j = 0 \tag{2}$$

with $(\delta\cdot)|_{j+1/2} = (\cdot)|_{j+1} - (\cdot)|_j$ and $(\mu\cdot)|_{j+1/2} = ((\cdot)|_j + (\cdot)|_{j+1})/2$. The fourth-order equivalent equation for (2) is

$$w_t + f_x(w) + (\delta x^2/6) f_{xxx}(w) = 0$$

where the last term represents a dispersive error. This term is corrected by replacing the third derivative with a centered second-order-accurate difference approximation. As a result, one obtains a fourth-order centered scheme. To ensure stability and avoid numerical oscillations, a dissipation term has to be added. A convenient choice is a scalar term of the form,[9] which is $O(\delta x^3)$ in smooth-flow regions: thus, the resulting numerical scheme is third-order accurate.

This scheme extends to the computation of flows with arbitrary equations of state in a straightforward manner; the main problem is to compute pressure and sound speed from the conservative variables. To do this, the temperature is first computed from internal energy and density using a Newton–Raphson iteration; then the pressure is computed from the thermal equation of state and the sound speed from

$$a = \frac{1}{\rho}\left[\frac{T}{c_v}\left(\frac{\partial p}{\partial T}\right)^2 + \rho^2\frac{\partial p}{\partial \rho}\right]^{\frac{1}{2}}$$

The numerical method is extended to multidimensional structured meshes through a cell-centered finite-volume formulation.[3,10] The numerical fluxes at cell interfaces are evaluated using weighted discretization formulas, accounting for mesh stretching and skewness: this ensures third-order accuracy on moderately deformed meshes and at least second-order on highly distorted meshes.

To evaluate the accuracy and efficiency of this scheme for dense gas computations, systematic comparisons are performed with an upwind scheme implemented within the same code. Specifically, Glaister's extension of Roe's scheme to real gases is considered,[4] with second-order MUSCL extrapolation and the Harten–Hyman entropy fix.

The proposed scheme is extended to the Navier–Stokes equations using a classical second-order centered approximation of the viscous fluxes. The solution is advanced in time using a four-stage Runge–Kutta scheme,[9] with local time stepping, implicit residual smoothing, and multigrid.

Results

Inviscid Transonic Flow past an Airfoil

Steady transonic inviscid flows over a NACA0012 airfoil at zero incidence are computed using three half-grids of 68×20, 136×40, and 272×80 cells, respectively. The outer boundary is 20 chords away from the airfoil, and the height of the first cell closest to the wall is about 5×10^{-3} chords on the medium grid.

The first test case concerns the flow of a perfect gas ($\gamma = 1.4$) with free-stream Mach number $M_\infty = 0.85$. The flow is characterized by strong shock waves at about 85% of the chord. The overall solutions of the centered and the upwind schemes (not shown for brevity) are quite similar and demonstrate the very good shock-capturing capabilities of both schemes. Analysis of the spurious entropy generation at the airfoil leading edge shows the very low intrinsic dissipation of the third-order scheme, whose numerical errors are up to one order of magnitude lower with respect to the upwind one.

Then two test-cases involving dense gas phenomena are considered. The working fluid is a BZT polytropic van der Waals gas ($\gamma = 1.0125$). The reduced thermodynamic freestream conditions are $p_\infty/p_c = 1.07$ and $\rho_\infty/\rho_c = 0.92$.

The DG1 test case has the same M_∞ as the preceding perfect-gas computation. However, for the considered BZT gas, Γ drops to negative values at the airfoil leading edge, and the flow remains subcritical. Figures 1a and 1b show pressure contours and pressure distribution at the wall, respectively. Both schemes give similar results. However, the third-order scheme produces entropy errors at the wall about one order of magnitude smaller than the upwind one (Fig. 1c).

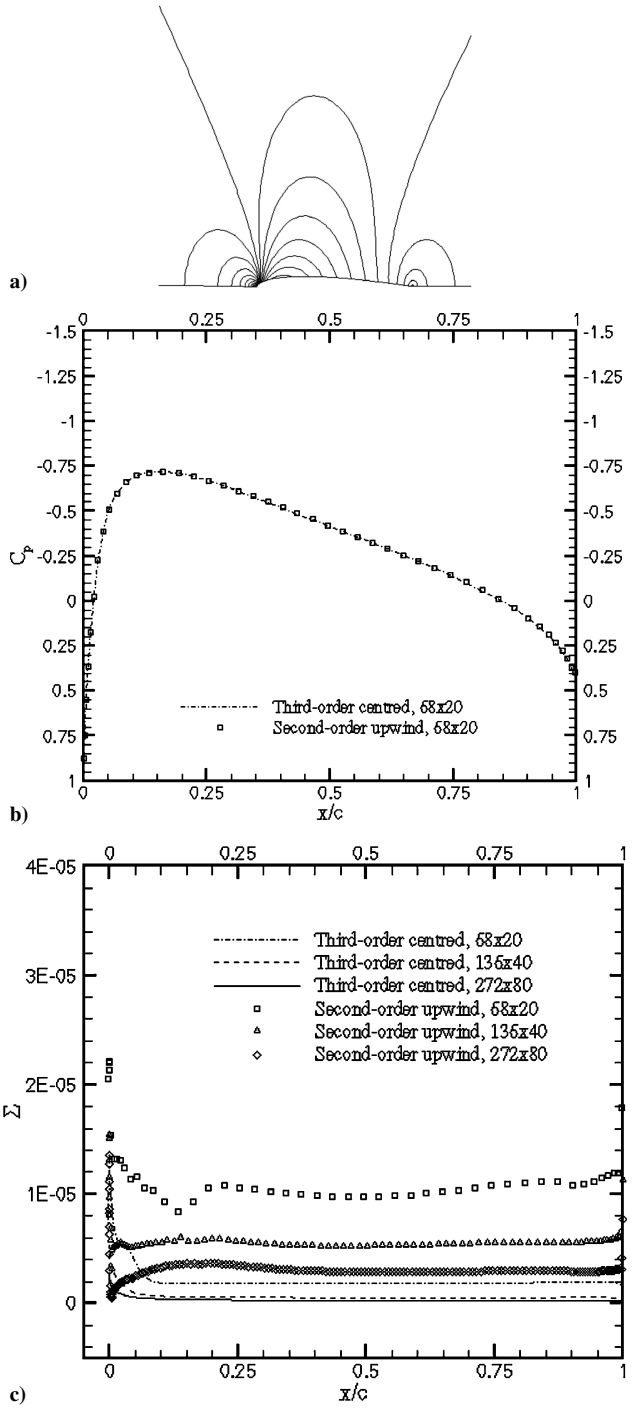

Fig. 1 Case DG1: a) isobars, $\Delta C_P = 0.05$ (fine grid); b) wall pressure; and c) entropy error at the wall.

In the DG2 test-case, M_∞ is increased to obtain supercritical flow. In such conditions, a very weak expansion shock forms at about 10% of the chord, followed by a weak compression shock at about 90% of the chord. Figure 2a shows pressure contours. The third-order scheme gives a slightly more diffused compression shock on the coarse grid, but better captures the suction peak after the expansion shock (Fig. 2b).

Similar computations have also been performed using the Martin–Hou equation of state. The working fluid is perhydrofluorene (commercial name PP10). Numerical results confirm the preceding

Table 1 Normalized CPU times

	Inviscid			Viscous turbulent	
Scheme	PFG	VDW	M-H	PFG	M-H
Third-order centered	1	1.17	2.67	1	2.34
Second-order upwind	1.22	1.50	4.72	1.19	4.05

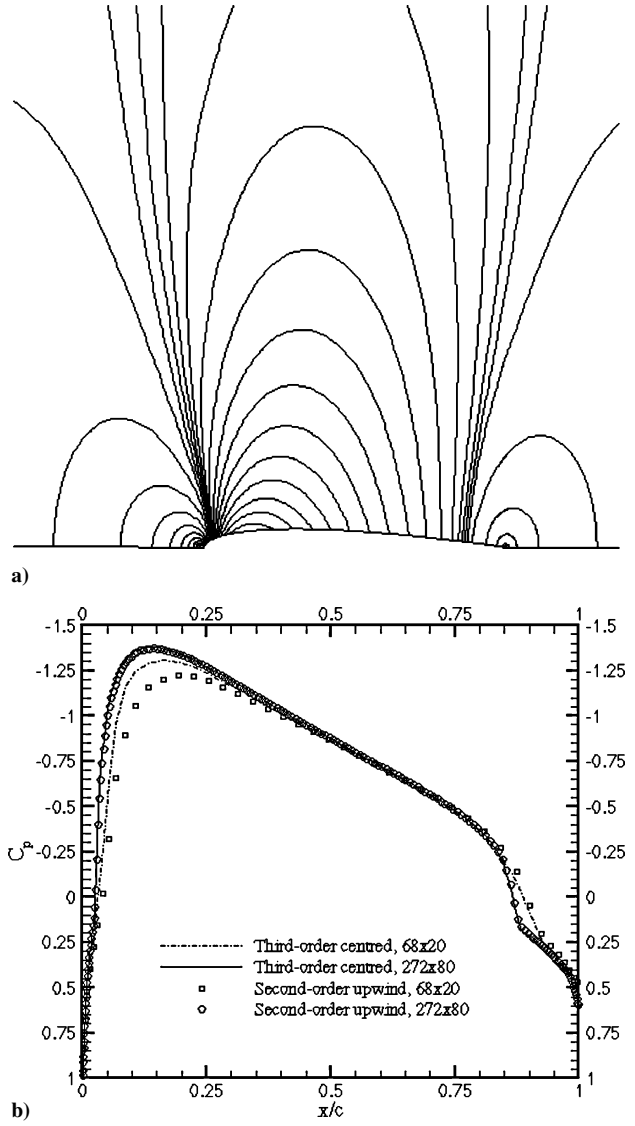

Fig. 2 Case DG2: a) isobars, $\Delta C_P = 0.05$ (third-order scheme, fine grid) and b) wall pressure.

considerations for the two schemes under analysis. Table 1 reports the normalized CPU times per iteration and per point (single grid). The centered scheme is about 28% cheaper than the upwind one when the van der Waals equation is used. However, the gain reaches 77% when the more complex Martin–Hou equation is used. Because the two schemes are of comparable accuracy, the centered scheme appears to be more advantageous for dense gas flow computations with complex EOS.

Laminar Flow over a Flat Plate

To validate the proposed method for viscous flow problems, the flow over a flat plate without pressure gradient is computed. The flow has $M_\infty = 0.2$ and $Re = 500$, based on inlet density and velocity and unit plate length. Results are computed in the rectangular domain $[0, 14] \times [0, 5]$, with the plate leading and trailing edges located at (1,0) and (13,0), respectively. A Cartesian grid

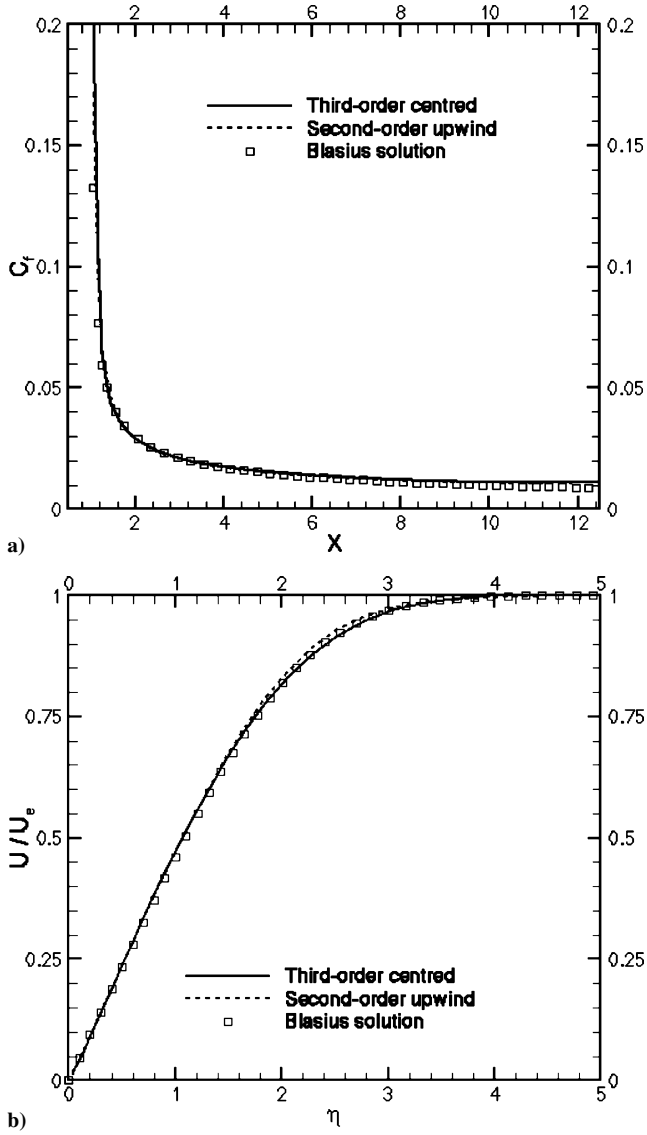

Fig. 3 Laminar flat-plate flow, $M_\infty = 0.2$: a) skin friction and b) velocity profile at midplate; comparison between two schemes.

of 140×50 cells, stretched in the direction normal to the wall, with first-cell height about 10^{-2}, is used. The plate wall is adiabatic. The numerical results are compared to Blasius's solution for incompressible boundary layers. The working fluid is PP10. Two operation points are considered: the first one lies in the dilute gas region ($\rho_\infty/\rho_c = 0.2$, $p_\infty/p_c = 0.6$), the second in the dense gas region, close to the $\Gamma = 0$ contour ($\rho_\infty/\rho_c = 0.571$, $p_\infty/p_c = 0.976$). In both cases, numerical results agree with theory, compressibility and dense gas effects being negligible. Figures 3a and 3b show skin friction distribution and velocity profiles for the two schemes: the results are very close to each other. The computed drag coefficients, 0.2290 and 0.2208 for the centered and the upwind scheme, respectively, compare well with the theorical value $C_D = 0.2057$. To explore dense gas effects, the flow is also computed at $M_\infty = 0.9$ and 2.0. At $M_\infty = 0.9$, results are still close to Blasius's solution, the coupling between the viscous and the thermal boundary layer remaining weak. At $M_\infty = 2$, friction heating becomes more significant, leading to a growth of boundary-layer thickness for the perfect gas; conversely, for the dense gas, the higher specific heat limits such growth, and the velocity profile remains quite closer to the incompressible one (Fig. 4).

Turbulent Flow past an Airfoil

The next test case concerns turbulent flow past a NACA0012 airfoil at $M_\infty = 0.8$, $Re = 9 \times 10^6$, and incidence 2.26 deg. The

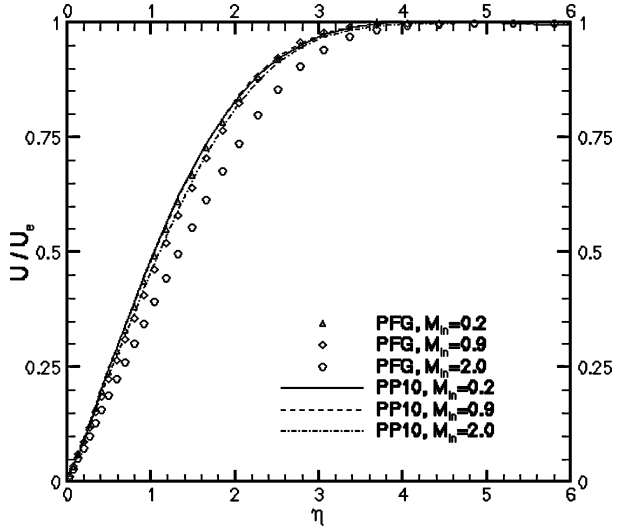

Fig. 4 Laminar flat-plate flow Mach number effect: comparison perfect gas/dense gas.

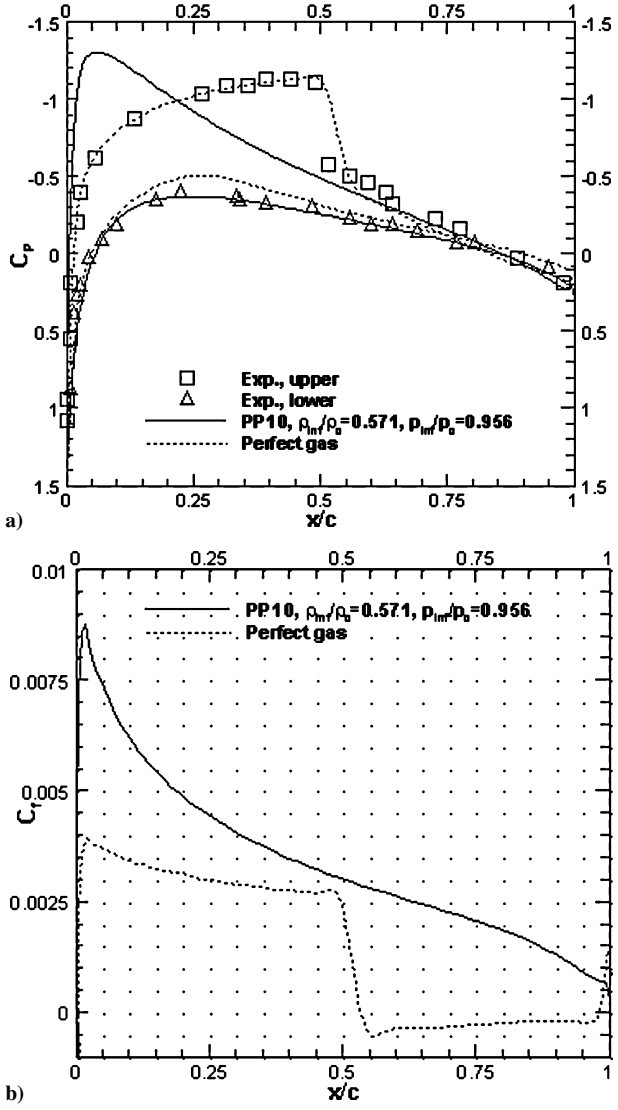

Fig. 5 Transonic turbulent flow past NACA0012: a) wall pressure and b) skin friction on upper surface.

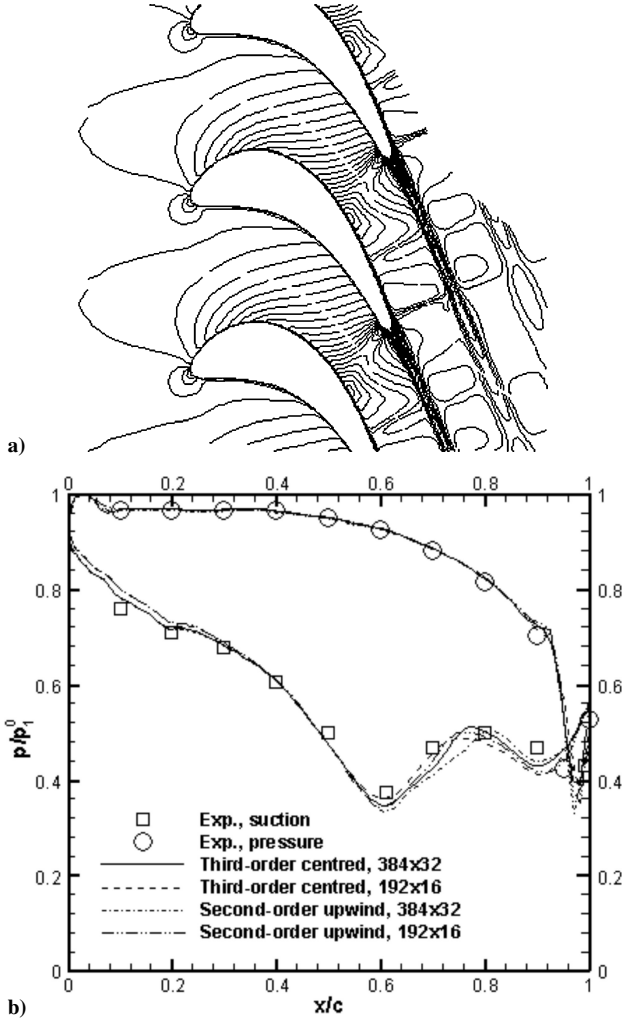

Fig. 6 VKI LS-59, perfect gas: a) Mach contours, $\Delta M = 0.05$ and b) wall pressure.

solution is computed on a C-grid of 256×64 cells, with mean $y^+ \cong 5$, outer boundary at 20 chords. The computed solution for perfect gas flow (wall pressure) is depicted in Fig. 5a. The flow is characterized by aftershock separation at the airfoil upper surface (Fig. 5b). The present results are in reasonable agreement with experimental data. Results for PP10 at $\rho_\infty/\rho_c = 0.571$, $p_\infty/p_c = 0.976$ ($\Gamma_\infty = -0.017$) are also provided: in the dense regime, the flow remains subcritical and separation is suppressed (Figs. 5a and 5b). Consequently, the drag coefficient drops from about 3.9×10^{-2} to 1.3×10^{-2}, whereas the lift coefficient grows from 0.33 to 0.37. Only minor differences (about 0.1% on lift and less than 1% on drag) exist between the two schemes considered: however, the centered scheme leads to considerable efficiency gains (up to 73%) over the upwind one (see Table 1).

Flow Through a Turbine Cascade

As a final application, transonic flow through the VKI LS-59 2D cascade (exit Mach equal to 1, inlet angle 30 deg, exit $Re\ 7.44 \times 10^5$) is computed, using C-grids of 192×16 and 384×32 cells. The perfect gas flow is characterized by a shock wave at half-chord and another shock attached to the trailing edge (Fig. 6a): both schemes provide results in good agreement with experimental data (Fig. 6b). Figures 7a and 7b show solutions for PP10 at inlet conditions $p_1/p_c = 1.08$, $\rho_1/\rho_c = 0.882$, $\Gamma_1 = 1.31$, with pressure jump through the cascade taken as in the perfect gas case: the first shock has almost disappeared and the trailing-edge shock is much weaker than in the preceding case.

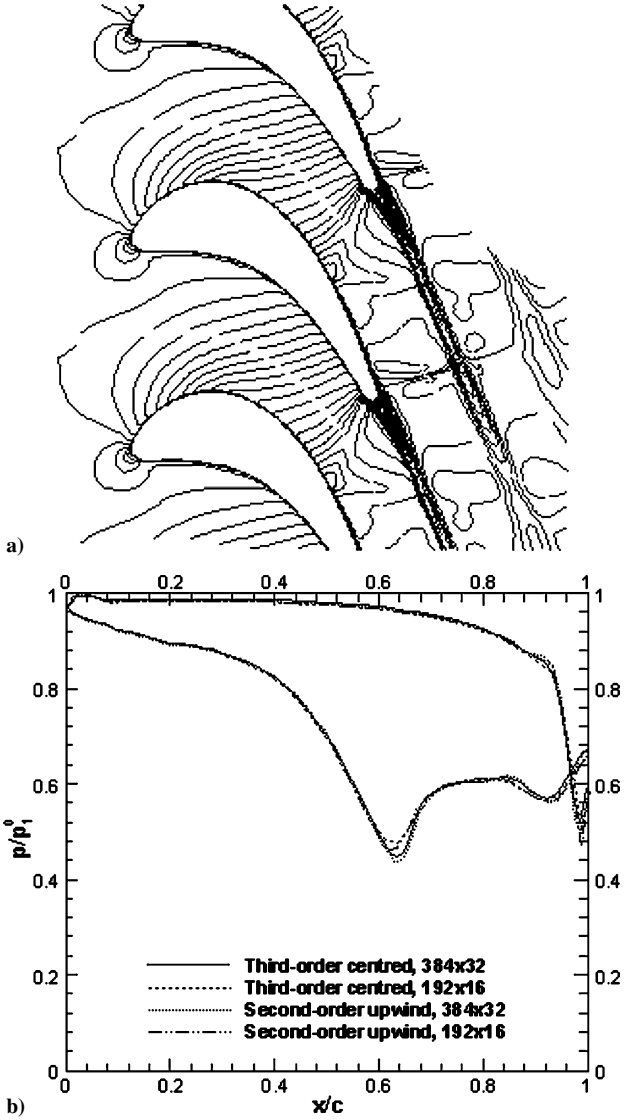

Fig. 7 VKI LS-59, dense gas: a) Mach contours, $\Delta M = 0.05$ and b) wall pressure.

Conclusions

In the present work, a high-order centered numerical method for dense gas flows has been proposed and validated. Results have been presented for several inviscid and viscous dense gas flows, and the proposed scheme has been systematicaly compared to a well-known second-order upwind scheme. The two schemes give results of comparable accuracy: the upwind scheme is slightly more accurate close to flow discontinuities, whereas the high-order centered scheme generates lower entropy errors at the leading edges of airfoils and blades. On the other hand, the centred scheme has lower computational requirements, with gains that become more significant when complex equations of state are considered.

References

[1]Cramer, M. S., "Nonclassical Dynamic of Classical Gases," *Nonlinear Waves in Real Fluids*, edited by A. Kluwick, Springer-Verlag, Berlin, 1991, pp. 91–145.

[2]Brown, B. P., and Argrow, B. M., "Application of Bethe–Zel'dovich–Thompson Fluids in Organic Rankine Cycles," *Journal of Propulsion and Power*, Vol. 16, No. 6, 2000, pp. 1118–1124.

[3]Huang, Y., Cinnella, P., and Lerat, A., "A Third-Order Accurate Centred Scheme for Turbulent Compressible Flow Calculations in Aerodynamics," *Numerical Methods in Fluid Dynamics*, Vol. 6, Will Print, Oxford, 1998, pp. 355–361.

[4]Glaister, P., "An Approximate Linearized Riemann Solver for the Euler Equations for Real Gases," *Journal of Computational Physics*, Vol. 74, No. 2, 1988, pp. 382–408.

[5]Martin, J. J., and Hou, Y. C., "Development of an Equation of State for Gases," *AIChE Journal*, Vol. 5, No. 2, 1955, pp. 142–151.

[6]Thompson, P. A., "A Fundamental Derivative in Gas Dynamics," *Physics of Fluids*, Vol. 14, No. 9, 1971, pp. 1843–1849.

[7]Cramer, M. S., and Kluwick, A., "On the Propagation of Waves Exhibiting Both Positive and Negative Nonlinearity," *Journal of Fluid Mechanics*, Vol. 142, 1984, pp. 9–37.

[8]Chung, T. H., Ajlan, M., Lee, L. L., and Starling, K. E., "Generalized Multiparameter Correction of Nonpolar and Polar Fluid Transport Properties," *Industrial and Engineering Chemistry Research*, Vol. 27, No. 4, 1988, pp. 671–679.

[9]Jameson, A., Schmidt, W., and Turkel, E., "Solutions of the Euler Equations by Finite Volume Methods Using Runge–Kutta Time-Stepping Schemes," AIAA Paper 8l-l259, June 1981.

[10]Rezgui, A., Cinnella, P., and Lerat, A., "Third-Order Finite Volume Schemes for Euler Computations on Curvilinear Meshes," *Computers and Fluids*, Vol. 30, Nos. 7–8, 2001, pp. 875–901.

H. Chelliah
Associate Editor